Int J Thermophys (2008) 29:1772–1784
DOI 10.1007/s10765-008-0447-4

Modeling of Transient Heat Transfer in Temperature Fixed Points: Indium Cell Design

V. Le Sant · R. Morice · G. Failleau

Published online: 5 June 2008

Abstract Laboratoire national de métrologie et d'essais has recently constructed a new device to realize the indium fixed point adiabatically. In parallel, a numerical heat transfer model has been developed as an aid to understanding its thermal behavior. This transient axially symmetric two-dimensional (2D) model simulates the melting process using the apparent specific heat method; the effects of mixing and convection within the liquid phase of indium are not taken into account. The thermal parameters, the nonuniformity of the furnace, and the thermal control of the surroundings were assessed with the aim of reducing parasitic heat exchanges. The results of the modeling are in good agreement with the measurements and clarify the parasitic heat flux observed during the phase transition. This article describes the model and the first results obtained. The model is a helpful tool in evaluating future technical improvements of the enclosure used to realize the indium fixed point.

Keywords Fixed point · Heat transfer · Indium · Modeling · Melting · Temperature

1 Introduction

Laboratoire national de métrologie et d'essais (LNE) has recently constructed and assessed a new experimental calorimeter to realize the indium fixed point adiabatically. The main objective is to reduce fixed-point realization uncertainties due to parasitic heat flux perturbing the temperature measurements during the phase transition. This experimental work [1] is the first step of a broader study for which a deep understanding of heat transfer is required. A numerical model was developed using

V. Le Sant (✉) · R. Morice · G. Failleau
Laboratoire national de métrologie et d'essais (LNE), Paris, France
e-mail: veronique.lesant@lne.fr

the commercial software Comsol to study heat transfer in temperature fixed points. The model is time dependent, based on the finite-element method.

The model is intended as an aid to identify the parasitic heat exchanges inside and outside the cell, to gain insight into the propagation of the solid/liquid interface, and to improve the design of the cell in consideration of the thermal conditions of its surroundings.

This article describes the model and its validation through a comparison to experimental data. A first assessment of thermal gradients along the thermometer and inside the cell is presented.

2 Principle and Description of the Calorimeter

The experimental setup consists of an indium cell surrounded by a separated external "guard" cell. Both are filled with indium. The whole system is placed in an air-flow furnace set at a temperature just below the phase transition of the metal. The energy required to melt both the cell and its guard is supplied by auxiliary heaters using heat pulses. Once on the phase transition, their temperatures are in extremely close agreement. The cell is melted adiabatically ('static' method), while the guard is continuously maintained in phase transition.

The enclosure is in the form of two graphite guard cells—a so-called main guard and a top guard (Fig. 1a)—filled with indium. The main guard is equipped with four auxiliary heaters. Another auxiliary heater is fixed to the top guard. The fixed-point cell consists of a PTFE crucible containing 0.316 kg of pure indium. Three auxiliary heaters are positioned along the cell crucible to melt the cell by heat pulses. The thermometer is composed of thin wires of platinum enclosed in a quartz sheath.

This setup also allows melting using the continuous heat flux method (dynamic method). In that case, the melt is initiated by first stabilizing the furnace a few degrees below the phase transition and then stepping the furnace temperature to a few degrees above and waiting for the metal to melt completely.

3 Numerical Model

3.1 Introduction

Experimental results obtained using the dynamic and static methods aid our understanding of the phase change process. Modeling the static and dynamic methods and comparing both models to the experiments constitute a robust validation.

This work models the melting of the indium cell using both methods. For the dynamic method, the guard is modeled as a block of high thermal conductivity (in this case, the indium from the guard is in the liquid state) when the cell starts melting. For the static method, the indium guard constitutes a wall at a constant temperature (the phase-transition temperature of indium).

Figure 1b shows the system modeled. It consists of four sub-domains: the fixed-point metal, the crucible, the main guard, and the platinum resistance thermometer (PRT). The thermal properties of indium, PTFE, and graphite used for the model are

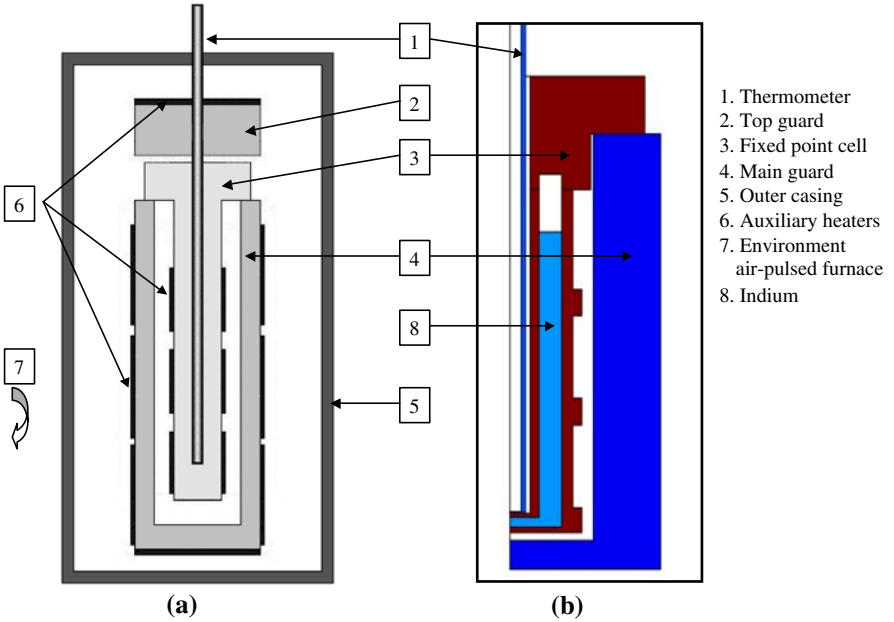

Fig. 1 (**a**) Schematic of the fixed-point cell developed at LNE and (**b**) schematic of the fixed-point cell modeled

Table 1 Thermal properties data used for the model

Thermal properties	Indium	PTFE	Graphite
Melting temperature (°C)	≈156.6 (156.5985 °C)		
Latent heat ($J \cdot kg^{-1}$)	28,500		
Heat capacity ($J \cdot K^{-1} \cdot kg^{-1}$)	243 (s)[a] 259 (l)[b]	1,000	690
Density ($kg \cdot m^{-3}$)	7,310 (s) 7,023 (l)	2,200	2,220
Conductivity ($W \cdot m^{-1} \cdot K^{-1}$)	81.8 (s) 42 (l)	0.25	160

[a] (s): solid state
[b] (l): liquid state

given in Table 1. The simplified design of the thermometer consists of a glass tube enclosing air and a central thin wire of platinum.

3.2 Assumptions

To simplify the system, certain assumptions, and approximations were made; these can be divided into three groups.

- *The first group of assumptions concerns the geometry of the cell.*

The model is two-dimensional (2D) with axial symmetry and calculated using cylindrical coordinates. The sub-domains are partitioned into triangular mesh elements, and the mesh is fixed; this results in an approximation because the mesh does not take the exact shape of the liquid–solid interface.

- *The second group of assumptions concerns heat transfer.*
  All heat is transferred by conduction inside the cell, the guard, and inside both phases of the metal. The PRT thermal model only takes into account exchange by conduction; the light-piping effect in the thermometer is neglected (the melting temperature of indium being low enough). The thermophysical properties of all parts of the system are considered constant.
- *The third group of assumptions relate to the phase transition of indium.*
  Indium is assumed to be pure and incompressible. Both phases are isotropic and homogeneous. There is no motion of metal (solid or liquid) inside the cell. The expansion of indium during the phase transition is neglected. The melting process is simulated by using the apparent heat-capacity method; the phase change occurs over a small temperature interval δT.

3.3 Boundary Conditions

The boundary conditions prescribed for the model are shown in Fig. 2. Figure 2a is used to model the phase change under continuous heat flux conditions (dynamic method); Fig. 2b is used to model the phase change of the indium cell under adiabatic conditions (static method). The boundary conditions are:

- Heat is exchanged between the furnace (set at a constant temperature of $T_{\text{melt}} + 3\,^{\circ}\text{C} = 159.6\,^{\circ}\text{C}$) and the outer wall of the main guard (diagram *a*); Heat is exchanged between the lateral guard (set at a constant temperature of $T_{\text{melt}} = 156.6\,^{\circ}\text{C}$) and the outer wall of the cell (diagram *b*);
- Fixed temperature on the upper boundary of the cell equal to the upper guard temperature (assuming perfect contact with the guard);
- Heat is exchanged on the top of the cell between the various surrounding environments (upper guard, furnace, and ambient air) and outer wall of the thermometer;
- Axial symmetry for all other boundaries;
- Thermal continuity between the different materials inside the cell.

The greatest difficulty of the modeling was to evaluate the heat exchange coefficients according to the rather complex shape of the cell and its surroundings (furnace, upper guard, lateral guard), taking into account radiative, convective, and conductive exchanges.

Practically, an estimate of the heat exchange coefficient between the lateral guard and the outer wall of the cell was carried out using the thermal resistance concept and assimilating the surroundings of the outer wall of the cell as a composite wall (i.e., air layer, guard, and outer casing as shown in Fig. 1). The overall heat transfer coefficient was determined from the sum of the thermal resistances (both series and parallel resistances) of the individual layers. An estimate of the heat exchange coefficient between the furnace and the outer wall of the main guard was done in the same way.

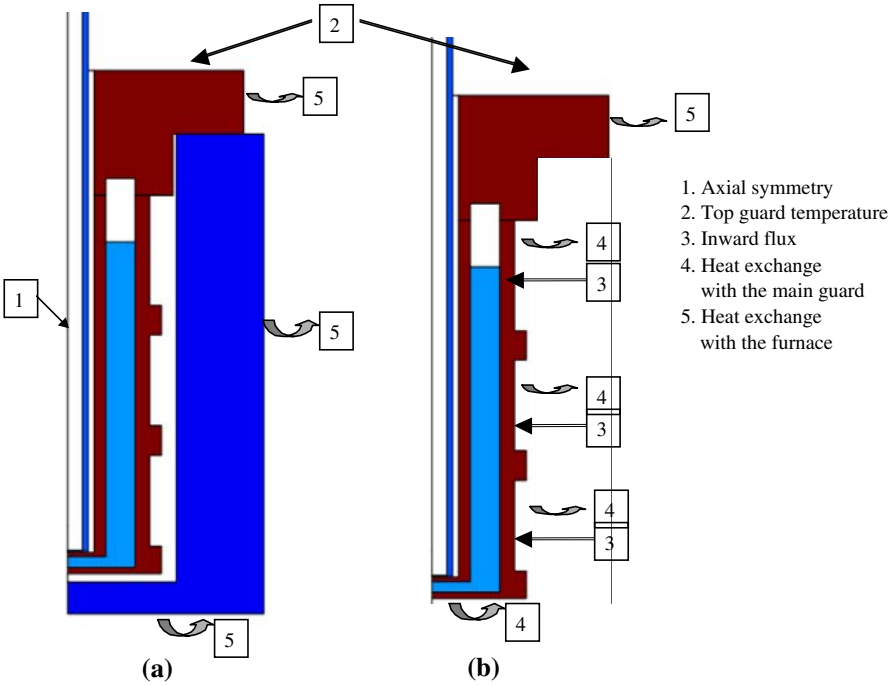

Fig. 2 (**a**) Schematic of the cell model with boundary conditions prescribed for the simulation of the "constant heat flux method," and (**b**) schematic of the cell model with boundary conditions prescribed for the simulation of the adiabatic method

3.4 Modeling of the Heat of Fusion by the Apparent Specific Heat Method

The heat of fusion is modeled by means of the apparent specific heat method. This is basically done by approximating the phase change at a fixed temperature through a gradual change of the specific heat over a small temperature interval [2].

Considering a 1D medium undergoing a phase change and assuming that the two phases, 1 and 2 (i.e., solid and liquid), are at thermal equilibrium during the phase change and all heat is transferred by conduction, then the governing heat equation inside the medium is given by Fourier's law:

$$C_{\mathrm{eq}}\frac{\partial T}{\mathrm{d}t} - k_{\mathrm{eq}}\nabla^2 T = 0 \quad \text{with } C_{\mathrm{eq}} = \rho_2 C_{p2} + f_1\left(\rho_1 C_{p1} - \rho_2 C_{p2}\right) + L\frac{\mathrm{d}f_1}{\mathrm{d}T}$$
$$\text{and } k_{\mathrm{eq}} = k_2 + (k_1 - k_2) f_1$$

This equation is called the apparent heat-capacity formulation. In this equation, C_{eq} denotes the apparent heat capacity, including the latent heat L for the change from phase 2 to phase 1 where f_1 is the volume fraction of phase 1, k_{eq} is the effective thermal conductivity, ρ_i is the density of phase i, C_{pi} is the specific heat capacity of phase i, and k_i is the thermal conductivity of phase i.

This formulation includes the latent heat of the phase change by means of a correction to the heat equation; the phase change is in fact treated as a nonlinearity of the thermal properties of the material [3]. On the other hand, this method needs to approximate the phase change at a fixed point by a gradual change over a small temperature interval, producing calculation errors for pure metal fixed points. Civan and Sliepeevich [2] have shown that the apparent heat-capacity method can produce acceptable results in the case of semi-infinite medium if $2\Delta T/|(T_i - T_s)| < 0.1$ where ΔT is the magnitude of the assumed temperature interval for the phase change and $(T_i - T_s)$ is the overall temperature variation of the system.

Practically, for a transition taking place at a fixed temperature, the volume fraction f_1 of phase 1 can be represented by a step function; its derivative $\frac{\mathrm{d}f_1}{\mathrm{d}T}$ is infinite at the transition temperature. To suppress this singularity, the apparent heat-capacity formulation uses a smooth function (Heaviside function, for example) to approximate f_1 over a finite temperature interval.

The apparent heat-capacity method allows for a simplified, continuous treatment of the system undergoing a phase change. In contrast, the classical formulation (Stephan problem) requires solutions of separate equations for each phase and another for the interfacial boundary.

Before implementing this formulation for the numerical model of the fixed-point cell, it was tested on a simplified model of a semi-infinite medium undergoing a phase change. Validation was done by comparison with the analytical solution of Neumann given in [4].

4 Comparison with Experimental Results

4.1 Introduction

To assess the model and adjust certain physical parameters, such as boundary conditions, simulation of the indium cell undergoing a phase transition and comparison with experimental data were carried out. Two kinds of simulation were considered: one called "the continuous heat flux method" and another, the "calorimetric method," as used in LNE experiments [1].

The input data used to run the model are given in Table 1, and the boundary conditions are those presented in Fig. 2. To maintain a reasonable computational time, the width of the transition pulse was fixed at $\delta T = 0.001\,^{\circ}\mathrm{C}$ and $\delta T = 0.0025\,^{\circ}\mathrm{C}$, respectively, for the simulation of the continuous heat flux method and for the simulation of the adiabatic method. These intervals constitute an artificial melting range compared to those of the pure indium metal (close to 0 °C) but are not too penalizing, as the results show.

4.2 Continuous Heat Flux Method

The continuous heat flux method consists of maintaining a constant temperature difference between the metal undergoing the phase change and its environment, throughout

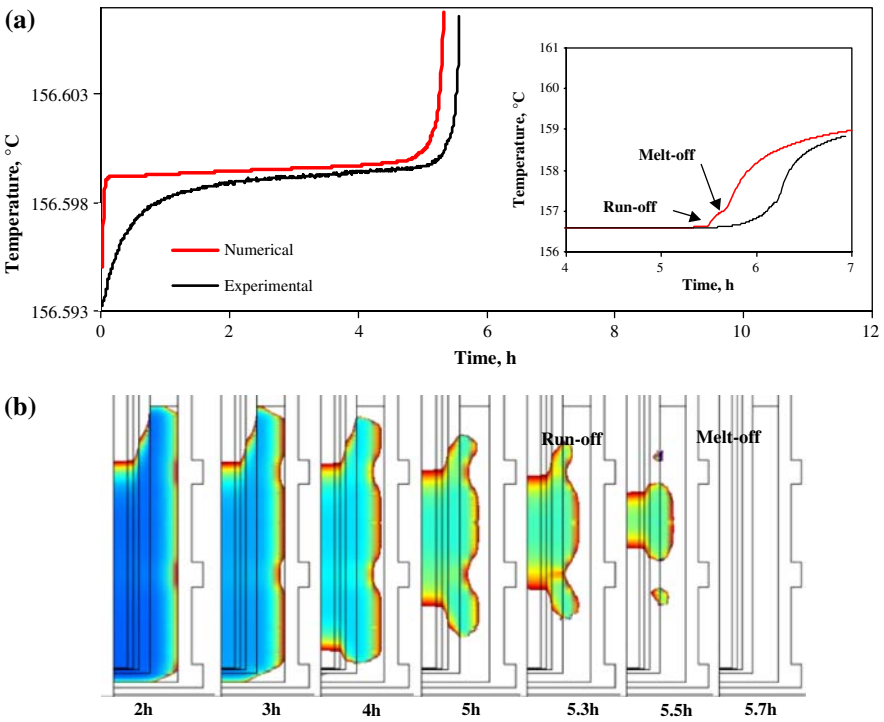

Fig. 3 (**a**) Comparison of melting curves obtained experimentally using the "constant heat flux method" and by computation and (**b**) evolution of the indium melt inside the cell using the "constant heat flux method"

the phase change. To enable a relevant comparison with experimental results, the temperature of the furnace has been identically adjusted above the melting temperature of indium. Three heat exchange coefficients were used for the computation ((6.0, 7.5, and 15) $W \cdot m^{-1} \cdot K^{-1}$) between the main guard and the furnace.

Figure 3a shows the temperature as measured and the temperature obtained by computation using the value 7.5 $W \cdot m^{-1} \cdot K^{-1}$; there is good agreement between experiment and simulation. In particular, the model shows a typical and well-known experimental phenomenon: near the end of the melt, the thermometer is strongly influenced by the temperature of the furnace, apparently "running-off" the melt even though some metal remains in the solid state. The melt of the last solid is observed as a "melt-off" following the "run-off" [5]. Figure 3b presents a 2D calculation versus time of the melting front in the cell, showing the large amount of unmelted metal at the "run-off" point.

The main differences between the numerical results and the experimental data are to be found at the beginning of the plateau. The main cause is the presence of impurities in the indium whereas the model considers ideally pure metal. In fact, as described by Ancsin [6] and Lee et al. [7], the purer the metal, the steeper the melting curve. Before putting forward impurities as the cause for differences near the beginning of the plateau, the temperature measured experimentally by a thermocouple fixed on

the external surface of the cell crucible was compared to the temperature determined by computation at the same location. Both showed equivalent behavior in reaching a constant temperature.

Differences between the numerical results and the experiments are notably attributable to the difficulty in estimating the heat transfer between the cell and its environment and to assumptions associated with the phase transition and the purity of the indium. Nevertheless, they are globally consistent with one another and the model is physically realistic.

4.3 Calorimetric Method

Once the guard begins melting ($T_{\text{guard}} = T_{\text{melt}}$), the cell is heated by discrete periodic pulses of energy supplied by auxiliary heaters mounted on the external surface of the cell crucible. Temperature measurements at the surface of the crucible are performed using Type K thermocouples attached to the auxiliary heaters.

A simulation was performed using the scheme of the cell presented in Fig. 2b. Three heat exchange coefficients were used for computation ((4.5, 6.2, and 9) $\mathrm{W \cdot m^{-1} \cdot K^{-1}}$) between the cell and the main guard to estimate the influence of radiative transfer, especially during the heating periods. For the computation, the experimental increases of the temperature of the main guard and the furnace were fitted by a Heaviside function.

Figure 4 superimposes numerical and experimental temperatures drawn from the solid-to-liquid phase change. Figure 4a presents the successive heat pulses observed with a Type K thermocouple on the external surface of the cell's crucible; there is good agreement with the numerical data for a heat exchange coefficient of $9\,\mathrm{W \cdot m^{-1} \cdot K^{-1}}$. Figure 4b compares the PRT's response with the temperature determined by computation for the same location at the bottom of the thermometer well.

The electrical power simulated in the model during the melting process does not match the real power supplied because of the difficulty in approximating the values of the heat exchange coefficients. We decided, as a simplification, to keep a constant power throughout the melt to observe the typical overheating near the liquidus point. On the other hand, the electrical power was experimentally controlled to avoid large temperature increases at the surface of the heaters in order to maintain the guard in phase transition. As shown in Fig. 4b, the platinum resistance thermometer readings are affected by the heat pulses when the thermometer well is no longer surrounded by a solid shell. The numerical results are consistent with the experimental results. In particular, it is remarkable to observe that the first heat pulse "seen" by the PRT appears in the simulation and in the experiments at the same point along the melt.

Experimentally, the operator uses a Type K thermocouple reading to detect locally the presence of the interface. Figure 5a superimposes the temperature measurement provided by a Type K thermocouple on the surface of one of the heaters for two different heating periods. The first one was observed during the melting process (presence of interface) and the second one at the end of the melting process. If an interface exists, the apparent heat capacity of the melting metal becomes very large and the measured temperature increases once the metal facing the thermocouple becomes completely liquid.

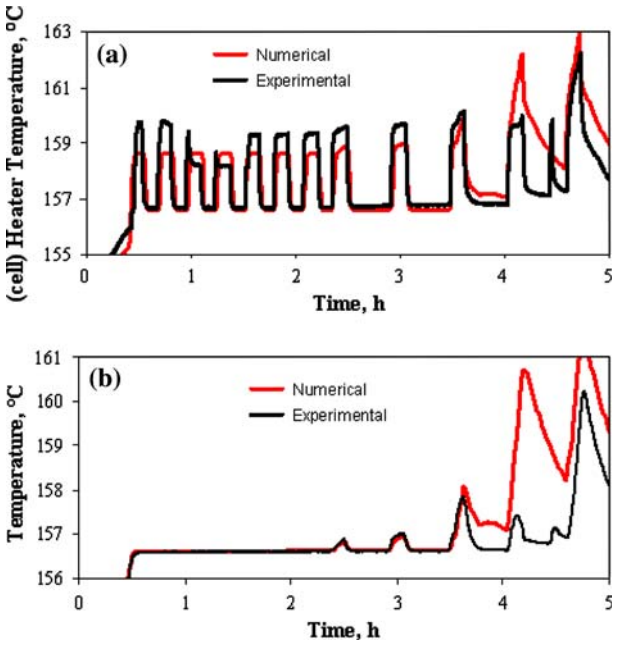

Fig. 4 (**a**) Comparison of experimental heat pulses with those obtained by computation and (**b**) comparison of melting curve obtained experimentally by the "adiabatic method" with one derived by computation

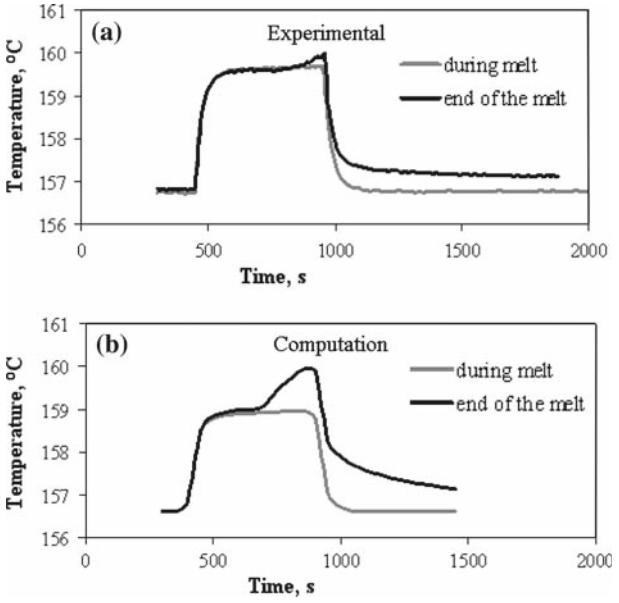

Fig. 5 (**a**) Evolution of pulses detected experimentally by a thermocouple and (**b**) evolution of pulses detected numerically at the location of the thermocouple

The numerical data shown in Fig. 5b validate that the presence of a liquid/solid interface can be checked from a temperature measurement done on the external surface of the cell crucible.

5 Parasitic Heat Flux

The modeling results have shed light on the remaining parasitic heat flux in the calorimeter. One of the detected defects is the lack of a lateral guard around the top of the cell as shown in Fig. 1a. This part of the cell is exposed to the furnace temperature, and therefore adiabatic conditions, are not realized. In fact, a thin conductive coating (of aluminum) covers the top of the cell, ensuring efficient thermal contact with the upper guard, and covers also the lateral part of the top of the cell. Consequently, it is at a temperature intermediate between the guard temperature and the furnace temperature, but close to the guard temperature as a result of the aluminum coating.

These imperfect adiabatic conditions near the top of the cell can easily be visualized in the 2D pictures drawn from the model in Fig. 6a. The radial effect is three times as important as the longitudinal effect. The graph in Fig. 6b showing the longitudinal gradient emphasizes that this thermal effect is only located over the top of the cell. Nevertheless, it is minor compared to the effect induced by the auxiliary heaters. Future improvement will require resolving this problem.

Another design defect identified is the presence of rings around the cell. They behave as fins and give rise to thermal gradients spreading over the cell to the thermometer well. Their presence affects directly the indium solid/liquid interface and, consequently, can be sources of error in the temperature measurements. The images presented in Fig. 7a were recorded during, and just after, a heating period. Figure 7b indicates the importance of the longitudinal gradient along the thermometer, especially during a heating period. Figure 7c shows that the cell requires about 1 h to re-equilibrate following a heat pulse. The limitations from the numerical model are obvious, numerical errors in the thermometer profile (curve following 60 min relaxation time) being of the order of the approximation attributable to the apparent specific heat equation.

Figure 8 illustrates the deformation of the liquid/solid interface as a function of time. The ingot does not melt homogeneously from the side. This is due to the absence of a continuous heater as well as to the nature of the crucible material (PTFE).

Some simulations were performed in order to evaluate the thermal effect generated by the heaters with respect to their position. Figure 9 highlights the importance of the position of the heater located closest to the position of the upper surface of the metal: overheating of the argon above the metal surface is avoided if the heater is positioned below the upper surface of the metal. Nevertheless, this effect is located far from the bottom of the cell well and should not disturb the temperature measurement.

6 Conclusion

The apparatus recently developed at LNE to realize the indium point by a calorimetric method has been modeled. The phase transition from solid to liquid was calculated

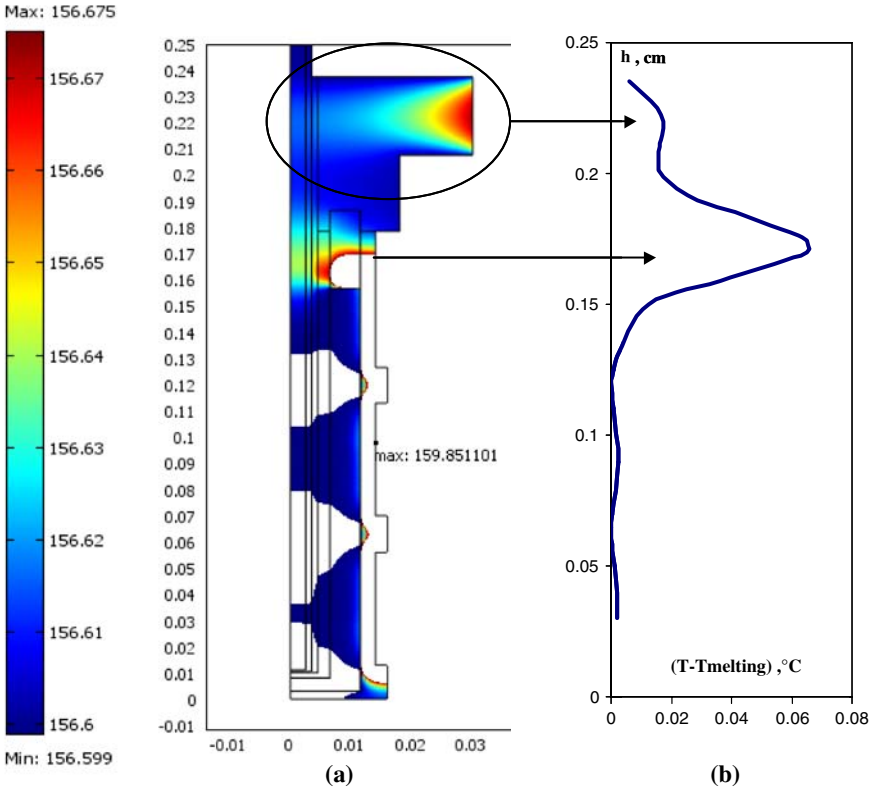

Fig. 6 (**a**) Thermal effect due to the lack of a lateral guard surrounding the top of the cell and (**b**) longitudinal gradient

for static (adiabatic) and also for dynamic (continuous heat flux method) melting conditions.

The main sources of error in the numerical model are poor knowledge of the heat transfer coefficients, the approximation of the phase change at a fixed temperature by a gradual change over a small temperature interval δT, the assumptions made (such as neglecting light-piping in the thermometer), the purity of the indium, the failure to consider motion of the solid or liquid inside the crucible, and numerical errors inherent to the finite-element method (mesh size, integration step). Concerning δT, the hardware used for the calculations did not allow it to be decreased to <1 mK.

Nevertheless, the model was not intended to estimate the uncertainties of temperature measurement. Rather, the purpose was to help in understanding the thermal behavior of the cell and in detecting the presence of thermal gradients within it. The experimental results validated both models, and the first calculated results have confirmed some modifications envisaged to improve the calorimeter.

At this stage, the model is being exploited to design a new indium fixed-point cell. Further modeling activities will concern the design of an adiabatic calorimeter to realize the aluminum fixed point.

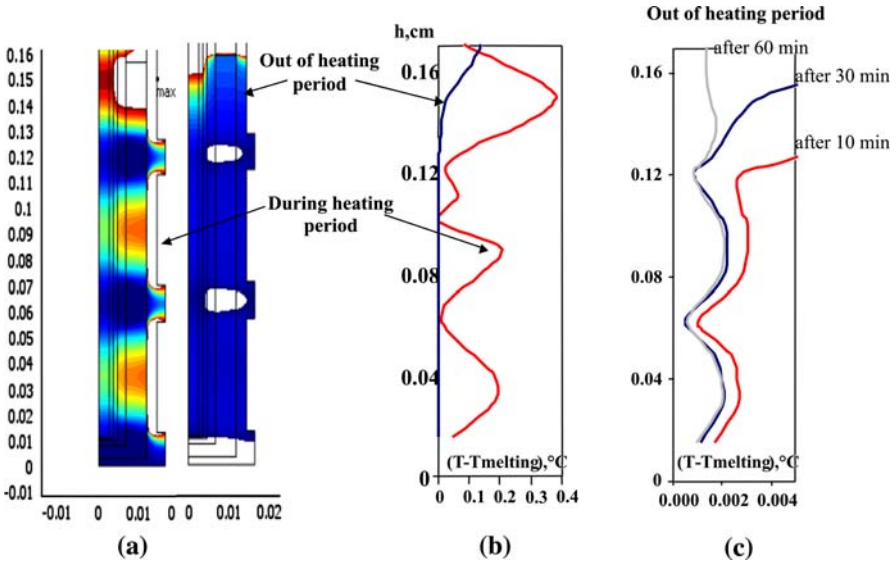

Fig. 7 (**a**) Thermal effect generated by the rings around the cell, (**b**) longitudinal gradient induced by the rings during a heating period and just after it, and (**c**) evolution of the longitudinal gradients induced by the rings outside the heating period as a function of time

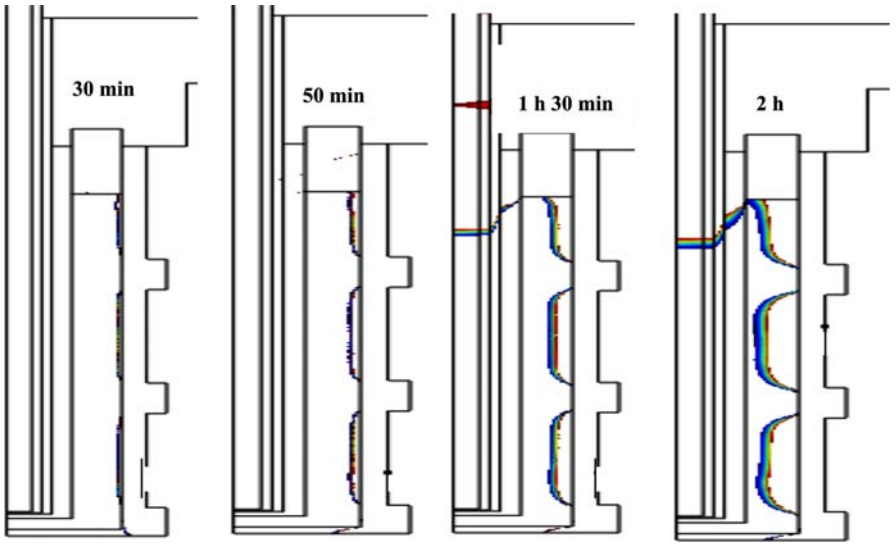

Fig. 8 Propagation of the liquid/solid interface as a function of time

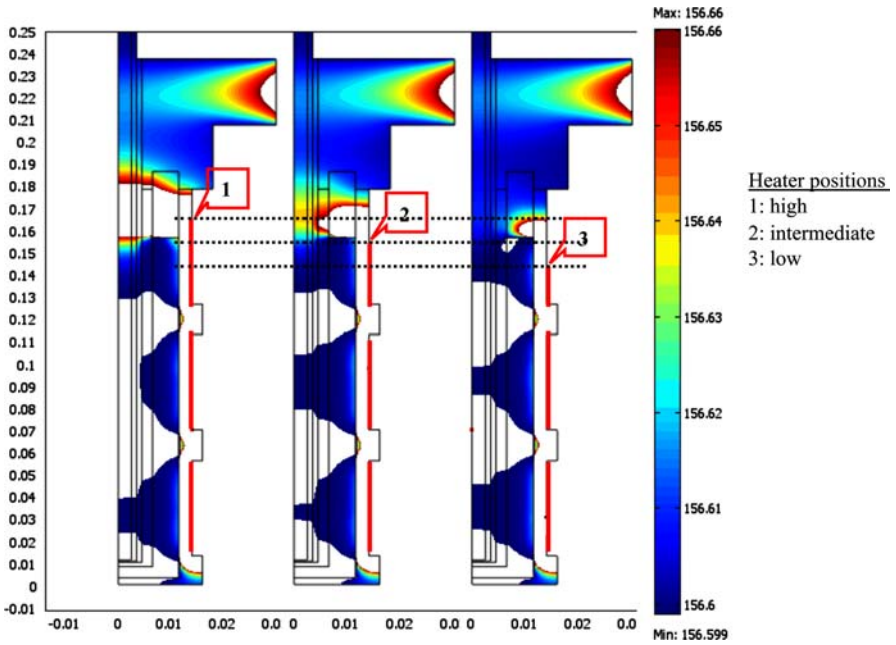

Fig. 9 Thermal effect caused by the position of the auxiliary heaters

References

1. R. Morice, G. Bonnier, J.C. Barbaras, N. Fleurence, V. Le Sant, P. Ridoux, J.R. Filtz, in *Proceedings of TEMPMEKO 2007*, *Int. J. Thermophys*., doi:10.1007/s10765-008-0445-6
2. F. Civan, C.M. Sliepeevich, Proc. Okla. Acad. Sci. **67**, 83 (1987)
3. J.M. Bergheau, R. Fortunier, *Simulation Numérique des Transferts Thermiques par Elements Finis* (Lavoisier Hermes Sciences, Paris, London, 2004)
4. H.S. Carslaw, J.C. Jaeger, *Conduction of Heat in Solids*, 2nd edn. (Clarenton Press, Oxford, 1959)
5. J. Ancsin, Metrologia **38**, 1 (2001)
6. J. Ancsin, Metrologia **21**, 7 (1985)
7. H.K. Lee, K.S. Gam, C. Rhee, Metrologia **28**, 413 (1991)